Electronic Materials Letters, Vol. 2, No. 2 (2006), pp. 95-100

Fabrication of Ni-Co Alloy Nanoparticles on a Polymer Film

Jung Hoon Kim, Jeon Kim, and Chong Seung Yoon*

Division of Materials Science and Engineering, Hanyang University, Seoul 133-791, Korea

A mono-layer of Ni-Co alloy nanoparticles was fabricated on a polyimide (PI) film via deposition of a 3.5-nm-thick Co thin film on top of preexisting nano-sized Ni particles followed by thermal annealing. The pre-existing 5-nm-sized Ni nanoparticles were produced on the PI thin film by imidizing a PI precursor layer with a $Ni_{80}Fe_{20}$ thin film on top of the precursor. The average particle size of the thus-fabricated Ni-Co alloy particles ranged from 5 nm to 9 nm depending on the heat treatment conditions. In general, the Ni-Co alloy particles exhibited a dramatic increase in saturation magnetization, particularly when the samples were annealed through rapid thermal annealing (RTA), as the thermal energy was efficiently delivered to the nanoparticles by RTA. The blocking temperature of the nanoparticles also increased to 230 K as Co was successfully incorporated into the Ni nanoparticles using RTA.

Keywords: nanoparticle, template, Ni-Co alloy, polyimide

1. INTRODUCTION

The recording density of conventional magnetic recording materials based on magnetic thin films is fast approaching the physical limit imposed by the superparamagnetic effect. As such, an alternative material system has been intensely sought after in order to overcome the random field fluctuation effect, which arises from thermal energy[1]. Lithographically patterned magnetic thin films[2-5] and self-assembled magnetic nanoparticle systems[6-8] have been considered as alternatives to replace the current high-density recording medium. Although both technologies hold great promise, to date, their successes have been limited to a laboratory scale. Furthermore, scale up of these technologies to an industrial scale is not likely to be realized in the near future. One of the main obstacles for a self-assembled magnetic nanoparticle system is that it lacks the robustness required for commercial applications. Because the magnetic particles are spatially separated and forced into a regular pattern based on relatively weak Van der Waal forces arising from the organic ligands[7,8], the system is inherently susceptible to thermal fluctuations.

We have recently reported on a mono-layer of magnetic particles embedded in a dielectric matrix[9-11]. These nanoparticles were magnetically isolated from one another while forming a mono-layer in a chemically stable polyimide (PI) matrix in the as-prepared state without requiring organic ligands to provide the necessary binding forces. The magnetic nanoparticles can be made from Ni or Fe_2O_3 whose average sizes ranged from 4 nm to 5 nm. However, because the average size is close to the superparamagnetic limit (~5 nm[12]), the magnetic moment for the particles is hardly detectable at room temperature. In this paper, we explore the possibility of increasing the magnetic moment at room temperature by alloying previously produced Ni nanoparticles with Co, which possesses much higher atomic magnetic moment than Ni (3.15 μ_B for Co versus 1.61 μ_B for Ni[13]). In addition, Co can form a solid solution with Ni throughout the nearly entire composition range[14]. We characterized the morphology and microstructure of the Ni-Co alloy nanoparticles and correlated these features to the magnetic properties of the nanoparticles.

2. EXPERIMENTAL PROCEDURE

Ni nanoparticles were produced on top of the PI film by depositing a thin $Ni_{80}Fe_{20}$ thin film on the PI precursor layer. During imidization of the PI precursor, Ni-rich nanoparticles were produced on the fully cured PI film. The PI precursor used in this experiment was p-phenylene biphenyltetracarboximide (BPDA-PDA) type polyamic acid (Dupont, PI2610D) dissolved in N-Methyl-2-Pyrrolidinone (1:3 ratio by weight). The polyamic acid (PAA) solution was spin coated onto a Si substrate having a 100-nm-thick thermal oxide layer. The thickness of the spin-coated PI precursor was controlled such that the final cured thickness of the PI layer was 40 nm. The PI precursor was subsequently treated at 135 °C for 30 min so as to evaporate the solvent. Using a DC magnetron sputterer, a 3.5 nm–thick $Ni_{80}Fe_{20}$ film was

*Corresponding author: csyoon@hanyang.ac.kr

deposited onto the PI precursor-coated substrate and the resulting $Ni_{80}Fe_{20}$/PI stack was cured at 400 °C for 1 hour under vacuum (10^{-3} Pa). In order to form the Ni-Co alloy particles, a thin Co film (3.5 nm thick) was deposited on top of the Ni particles and heat treated at two different temperatures (400 °C and 600 °C) for 1 hour under vacuum using a conventional furnace and rapid thermal annealing (RTA) at the same temperatures for 30 sec. RTA was performed using three 500 W halogen lamps. Transmission electron microscopy (TEM, JEOL 2010) was used to characterize the synthesized nanoparticles while monochromatic X-rays generated from Al Kα (15 kV) were used for x-ray photoelectron spectroscopy (XPS, PHI 5600). Magnetic measurements were performed using a superconducting quantum interference device (SQUID).

3. RESULTS AND DISCUSSION

3.1. Particle morphology and structure

Figure 1 shows TEM plan view images of the Ni nanoparticles prior to the Co deposition and after a thin film of Co (3.5 nm thick) was deposited on top of the nanoparticles. A comparison of the two images in Fig. 1 reveals that, instead of forming a continuous film over the preexisting Ni nanoparticles, ~10 nm-sized discrete Co islands cover the Ni particles, because Co nucleated preferentially on the preexisting metal particles during deposition. The electron diffraction pattern of the inset in Fig. 1(b) indicates that the deposited Co film retained the fcc structure, isostructural with the preexisting Ni nanoparticles. It is conjectured that this discontinuous microstructure of the deposited Co film encapsulating the Ni nanoparticles should shorten the diffusion length and expedite the formation of a Ni-Co solid solution while reducing the probability of forming separate Co clusters during thermal treatment. Energy-dispersive x-ray spectroscopy analysis of the thin film confirmed that the sample contained Co and Ni in a nearly equi-atomic ratio.

Figs. 2(a) and (b) show images of the nanoparticles fabricated by thermally annealing the sample in Fig. 1(b) in a conventional tube furnace at 400 °C and 600 °C, respectively. Average particle size and areal density for the nanoparticles were estimated from the TEM micrographs and are summarized in Table I. Compared to the nearly spherical Ni particles observed in our previous work[10], these alloy nanoparticles are rather irregularly shaped with a relatively large particle size distribution, especially for the alloy particles produced at 600 °C, as can be seen from Fig. 2(b). The average particle size for both samples annealed at 400 °C and 600 °C were considerably larger than that of the Ni nanoparticles prior to the Co deposition, which were only 4.5 nm in diameter[15]. The increased average particle size suggests that the deposited Co was indeed incorporated into the pre-existing Ni particles during annealing. When heat treated at 600 °C, the nanoparticles grew even larger, to 9.2 nm, due to coarsening. In comparison, when the samples were heat treated by RTA, the particles also became larger in size compared to the pre-existing Ni nanoparticles, but no essential difference in particle morphology was observed between samples annealed at 400 °C and 600 °C. Notably, the average particle size for the sample annealed by RTA at 600 °C was slightly smaller than that for the sample annealed at 400 °C, in contrast to the samples annealed using a conventional furnace. The histrograms shown in Fig. 3 better demonstrate the difference in the particle size distributions. While there was no significant difference between the two RTA samples, the distribution curve for the sample annealed in the furnace at 600 °C contains a broad shoulder near 13 nm due to coarsening, which substantially raised the average particle size for the sample. In contrast to the slow conventional furnace thermal treatment, RTA typically generates intense heat that is

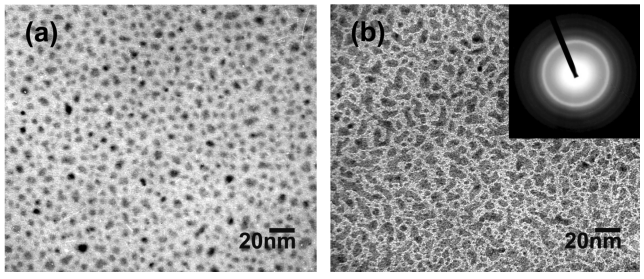

Fig. 1. TEM plan view images: (a) Ni nanoparticles formed on PI film by thermal imidization of $Ni_{80}Fe_{20}$ (3.5 nm)/PAA at 400 °C prior to Co deposition, (b) Co-Ni nanoparticles after depositing a 3.5-nm-thick Co film of 3.5-nm-thick on the Ni nanoparticles. The inset shows the corresponding electron diffraction pattern.

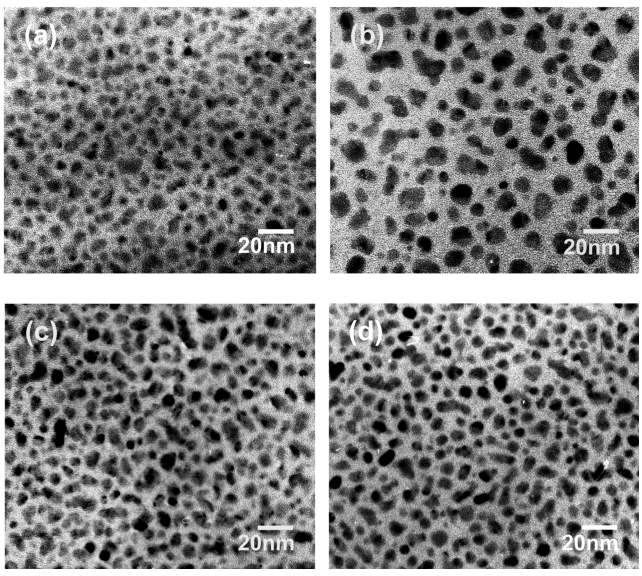

Fig. 2. TEM plan view images of Ni-Co alloy nanoparticles fabricated by heat-treating the sample in Fig. 1(b): (a) conventional tube furnace at 400 °C, (b) furnace at 600 °C, (c) RTA at 400 °C, (d) RTA at 600 °C.

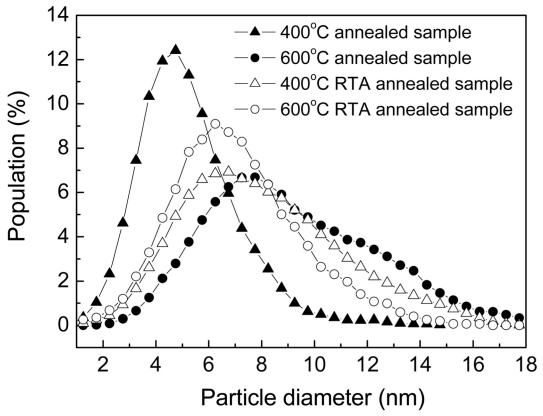

Fig. 3. Particle size distributions for Ni-Co alloy nanoparticles fabricated under different heat treatment conditions.

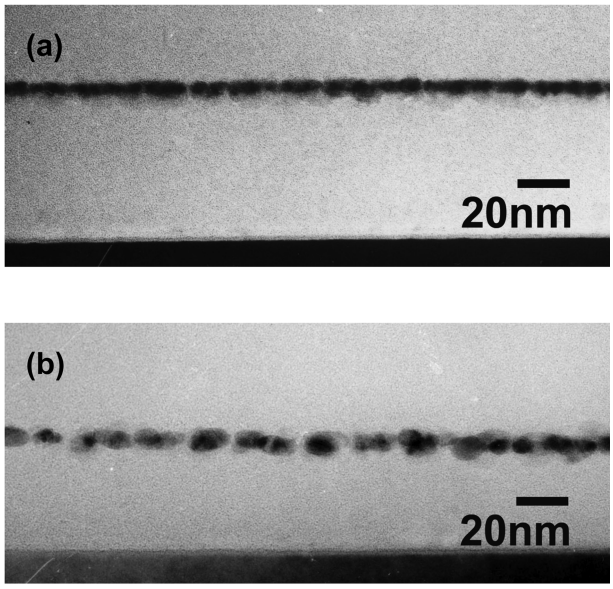

Fig. 4. Cross-sectional TEM images of the furnace-treated samples: (a) at 400 °C, (b) at 600 °C.

Table 1. Average particle size, particle size distribution, and areal density for the Ni-Co alloy nanoparticles produced at different temperatures by furnace annealing and RTA

Temperature	Average particle diameter (nm)	Areal density (%)
400 °C, furnace	5.2 ± 1.8	30
600 °C, furnace	9.2 ± 3.4	33
400 °C, RTA	8.5 ± 3.4	45
600 °C, RTA	7.1 ± 2.8	37

mainly concentrated at the surface, a process that is also aided by the poor thermal conductivity of PI[16]. RTA is therefore more effective in terms of providing mobility to the

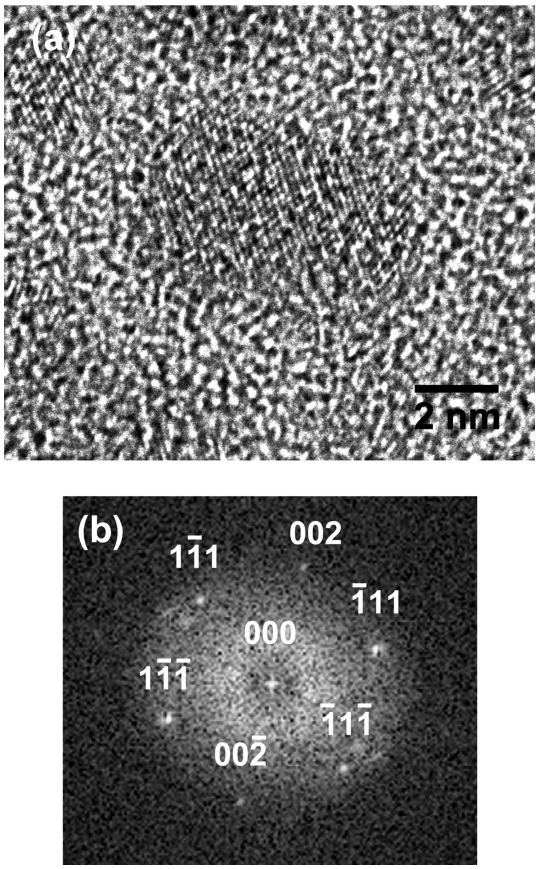

Fig. 5. (a) High-resolution TEM image of Ni-Co nanoparticles fabricated by furnace-treatment at 400 °C, (b) indexed Fourier transform of (a).

metal atoms residing on the top surface, thus enabling them to coalesce into Ni-Co solid solution particles. In addition, the extremely short period during which RTA was carried out essentially prevented the coarsening of the particles regardless of the annealing temperature. As for the areal density of the Ni-Co alloy nanoparticles, the values listed in Table 1 are substantially higher than that previously measured for the Ni nanoparticles (24 %), as would be expected from the incorporation of extra material into the particles.

Figure 4 shows cross-sectional TEM images of the furnace-treated samples at 400 °C and 600 °C. As can be seen in these images, the mono-layer structure of the pre-existing Ni nanoparticles was maintained during the heat treatment process up to 600 °C, at which the PI structure has been previously observed to be severely damaged[17]. Fig. 5 (a) shows a high-resolution TEM image of the Ni-Co nanoparticles obtained from the furnace-treatment at 400 °C. Well-resolved lattice fringes indicate that the particles were well crystallized. The corresponding Fourier transform of the image shows the particle is aligned along the [110] direction and verifies that the individual particle is indeed single-phased containing no other secondary structures.

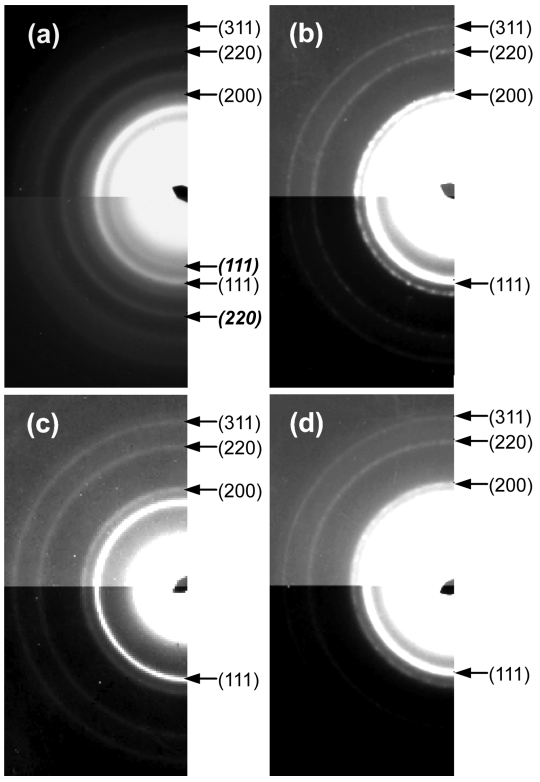

Fig. 6. Indexed electron diffraction patterns of nanoparticles produced from different heat treatments: (a) furnace-annealed at 400 °C, (b) furnace-annealed at 600 °C, (c) RTA at 400 °C, (d) RTA at 600 °C.

Shown in Fig. 6 are respective selected area electron diffraction patterns obtained from the samples. Except for the sample that was furnace-heat treated at 400 °C, in all samples the nanoparticles were single-phased with a fcc structure. The sample furnace-heat treated at 400 °C, as indicated in the diffraction pattern, contained a ring corresponding to the (111) peak of CoO. Notably, the XPS spectrum obtained near the Co L- absorption in Fig. 7 was in agreement with the electron diffraction result that Co in the sample furnace-heat treated at 400 °C was partially oxidized. Both $2p_{3/2}$ and $2p_{1/2}$ peaks in the XPS spectrum for this sample, shown in Fig. 7(a), had a doublet structure. A small $2p_{3/2}$ peak at 778.3 eV [18, 19] precisely matched the binding energy of metallic Co with the main $2p_{3/2}$ peak near 780 eV corresponding to the Co-oxide binding energy[19]. The peak separation clearly shows that Co was partially oxidized for this sample. The relative peak intensity suggests that a major fraction of Co atoms were in an ionized state. On the other hand, the sample that was furnace-heat treated at 600 °C exhibited a single $2p_{3/2}$ peak at 778.3 eV with a barely noticeable oxide shoulder at 780 eV, as can be seen from Fig. 7(b). The XPS analysis from both RTA samples (not shown) also exhibited spectra similar to those shown in Fig. 7(b). It appears that the Co thin film was partially oxidized during the furnace-heat treatment at 400 °C, possibly from reaction with the residual PAA that may have not been fully imidized during the initial

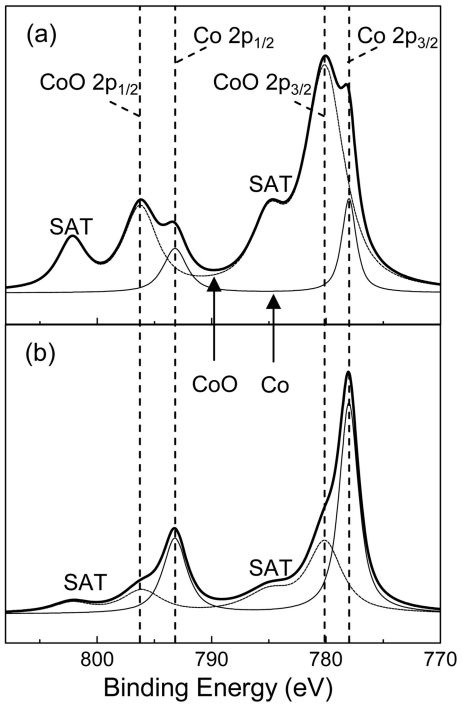

Fig. 7. Co 2p XPS spectra of furnace-treated Ni-Co alloy nanoparticle samples with the peak separated curves showing contributions from CoO and Co : (a) at 400 °C, (b) at 600 °C.

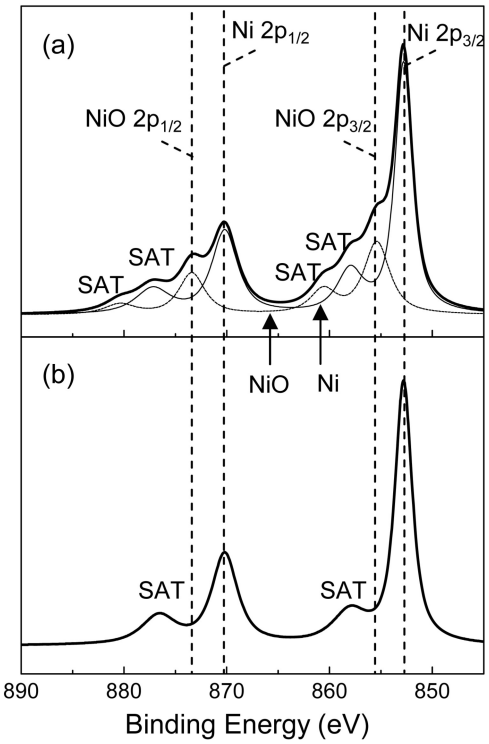

Fig. 8. Ni 2p XPS spectra of furnace-treated Ni-Co composite nanoparticle samples with the peak separated curves showing contributions from NiO and Ni: (a) at 400 °C, (b) at 600 °C.

curing process. For the RTA samples, it is plausible that the intense heat lasting for only a short period (30 sec) minimized the chemical reaction of Co on the surface with the PI matrix. For the sample that was furnace-heat treated at 600 °C, one would expect a larger fraction of Co to be oxidized compared to the sample annealed at 400 °C. The contrary evidence in Figs. 6 and 7 may be attributed to the destruction of the chemical structure of PI at this temperature, accompanied by evolution of reducing chemical complexes. More convincing evidence of reduction of metal ions can be seen in Fig. 8, which shows changes in the chemical state of Ni, as determined using XPS.

The Ni 2p absorption edge from the sample that was furnace-treated at 400 °C, shown in Fig. 8 (a), suggests that Ni remained mostly metallic. Both the Ni 2p binding energy (852.7 eV) and the energy width between the $2p_{3/2}$ and $2p_{1/2}$ peaks matched well with the standard values for metallic Ni [18,20]. However, the spectrum also contained weak shoulders arising from the presence of NiO. From the peak separation and the comparison of the relative peak intensity, it was found that the mole fraction ratio, X_{Ni}/X_{Ni2+}, was ~ 0.2. A similar XPS analysis of the as-prepared Ni nanoparticles prior to the Co deposition also showed that X_{Ni}/X_{Ni2+} was ~ 0.1[11]. Similar to Co, Ni in the preexisting nanoparticles was further oxidized by subsequent annealing. However, the Ni spectrum from the sample annealed at 600 °C (Fig. 8(b)) and the RTA samples (not shown) matched that of a pure metallic Ni film without exhibiting any evidence of the presence of Ni oxides.

3.2. Magnetic properties

Figure 9 shows magnetic hysteresis loops from the furnace-annealed samples measured using SQUID at room temperature. The nanoaparticles from the sample annealed at 400 °C were ferromagnetic with the magnetization saturating near 700 Oe. However, the magnitude of the saturation magnetization rose only slightly above that of the preexisting Ni nanoparticles in spite of the Co incorporation. This is attributed to the oxidization of a large fraction of Co atoms to become CoO, which is an antiferromagnet near room temperature (Neel temperature = 290 K[21]). The magnetization curve for the sample exhibited a noticeable rise in coercivity, which was absent from the Ni nanoparticles. The relatively large coercivity likely arose from the exchange bias between the antiferromagnetic CoO and residual Co or Ni[22]. Meanwhile, the Ni-Co alloy particles produced at 600 °C exhibited a marked increase in the saturation magnetization compared to the Ni nanoparticles, evincing that Co was successfully incorporated into the Ni nanoparticles. In addition, the larger volume fraction of ferromagnetic materials in the 600 °C-annealed sample and subsequent increase in magnetic interactions among particles led to increased initial susceptibility and a considerable decrease in the saturation field of the magnetization curve compared to the initial Ni nanoparticles[23]. Shown in Fig. 9(b) are hysteresis loops obtained from

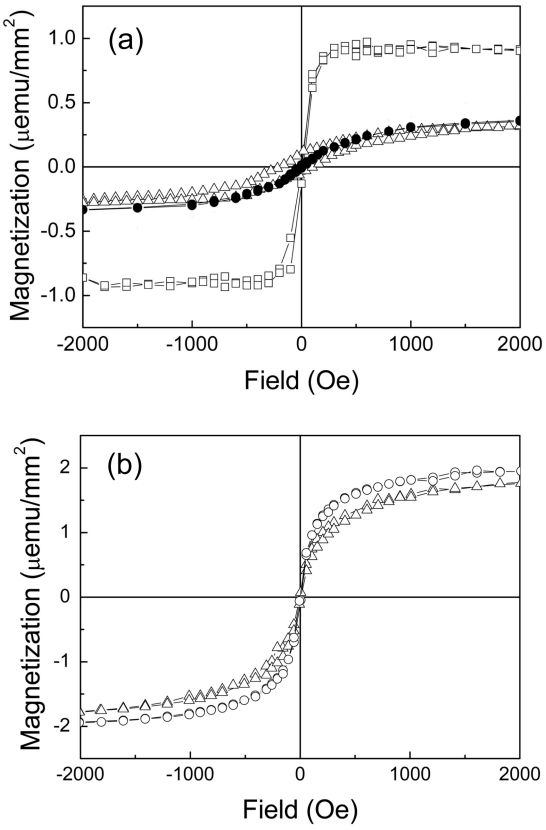

Fig. 9. Magnetic hysteresis loops from different Ni-Co alloy nanoparticle samples measured using SQUID at room temperature: (a) furnace-annealed samples (△: at 400 °C, □: at 600°C, ●: Ni nanoparticles before the Co deposition), (b) RTA-treated samples (△: at 400°C, ○: at 600 °C).

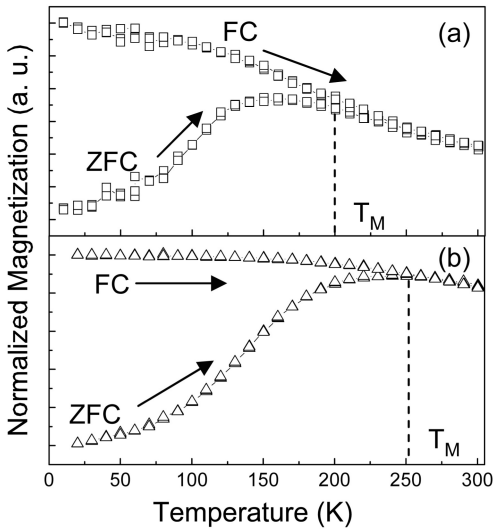

Fig. 10. ZFC and FC curves of Ni-Co alloy nanoparticle samples: (a) furnace-annealed at 400 °C, (b) RTA at 600 °C.

the two RTA samples at room temperature. The increase in the saturation magnetization is more dramatic for these samples, nearly quadrupling in magnitude, compared to the initial Ni nanoparticles. As observed in the particle morphology and microstructure, no essential difference in magnetic properties was observed between these two samples treated by RTA, regardless of the annealing temperature.

In Fig. 10, we plotted the temperature dependence of the magnetization measured with an applied field of 50 Oe for both field cooled (FC) and zero field cooled (ZFC) samples. The ZFC curve for the sample treated by the conventional furnace at 400 °C in Fig. 10(a) decays uniformly and joins the FC curve near its peak with the blocking temperature, T_B of 150 K. The ZFC and FC curves closely resemble those of the Ni nanoparticles produced by magnetron sputtering with an average particle size of 10 nm and T_B of ~ 240 K[24]. The ZFC and FC curves for the Ni-Co nanoparticles produced by RTA at 600 °C also showed similar behavior; however, the blocking temperatures increased to 230 K, which amounts to a ~ 50 % increase. Since T_B; (E_a + E_{int}), where E_a is the magnetocrystalline anisotropy energy and E_{int} is the dipole field energy[23], the increase in T_B can be traced both to the increase in E_a by Co incorporation[25] and to the increase in E_{int} due to the increased particle density[23].

In general, the measured magnetic properties correlated well with the observed morphology and microstructure of the alloyed nanoparticles. It was also demonstrated that RTA was more effective in fabricating alloyed Ni-Co nanoparticles compared to the conventional furnace treatment, as the thermal energy was efficiently delivered to the nanoparticles by RTA.

4. CONCLUSION

We demonstrated that a mono-layer of Ni-Co alloy nanoparticles can be fabricated via deposition of a thin film of Co on top of preexisting nano-sized Ni particles, followed by thermal annealing. Thus-fabricated Ni-Co alloy particles exhibited a dramatic increase in saturation magnetization, especially when the samples were annealed using RTA. Based on our results, it is speculated that the magnetic properties of the alloy nanoparticles can be further improved by repeated Co deposition and RTA so as to increase the saturation magnetization while the coercivity can also be increased by incorporating a thin CoO layer into the nanoaparticles to induce exchange bias.

ACKNOWLEDGMENTS

This work was supported by the Ministry of Science and Technology through the Nanoscopia Center of Excellence at Hanyang University and also partially supported by the research fund of Hanyang University (HY-2002).

REFERENCES

1. M. L. Plumer, J. van Ek, and D. Weller (eds.), *The Physics of Ultra-High-Density magnetic Recording,* p. 34, Springer-Verlag, Berlin (2001).
2. C. A. Ross, S. Haratani, F. J. Castano, Y. Hao, M. Hwang, M. Shima, J. Y. Cheng, B. Vogeli, M. Farhoud, M. Walsh, and H. I. Smith, *J. Appl. Phys.* **91**, 6848 (2002).
3. Navab Singh, S. Goolaup, and A. O. Adeyeye, *4th IEEE conference on nanotechnology,* p. 55, Munich, Germany (2004).
4. Takumi Sannomiya, Ji Shi, Yoshio Nakamura, and Osamu Nitto, *J. Appl. Phys.* **96**, 5050 (2004).
5. J. S. Bradley and G. Scgmid, in: G. Schmid (eds.), *Nanoparticles: From theory to application,* p.186, Wiley-VCH Verlag GmbH & Co. KGaA, Weinheim (2004).
6. J. W. Harrel, S. Wnag, D. E. Nikles, and M. Chen, *Appl. Phys. Lett.* **79**, 4393 (2001).
7. C. Petit, A. Taleb, and M. P. Pileni, *J. Phys. Chem B.* **103**, 1805 (1999).
8. J. N. Park, Eunae Kang, S. U. Son, H. M. Park, M. K. Lee, J. H. Kim, K. W. Kim, H. J. Noh, J. H. Park, C. J. Bae, J. G. Park, and T. G. Hyeon, *Adv. Mater.* **17**, 249 (2005).
9. S. K. Lim, K. J. Chung, Y-H. Kim, C. K. Kim, and C. S. Yoon, *J. Colloid Interface Sci.* **273**, 517 (2004).
10. S. K. Lim, C. S. Yoon, C. K. Kim, and Y. H. Kim, J. Phys. Chem. B **108**, 18179 (2004).
11. S. K. Lim, I. S. Chun, K. S. Ban, C. S. Yoon, C. K. Kim, and Y. H. Kim, *J. Colloid Interface Sci.* **295**, 108 (2006).
12. Allan H. Morrish (eds.), *The Physical Principles of Magnetism,* p. 362, *IEEE Press*, Piscataway, New Jersey (2001).
13. H. P. J. Wijn (ed.), *Magnetic Properties of Metals: d-Elements, Alloys and Compounds,* p.8, Springer-Verlag, Berlin (1991).
14. A. Fernandez Guillermet, *Z. Metalldke,* **78**, 639 (1987).
15. J. W. Kim, S. K. Lim, C. K. Kim, Y. -H. Kim, and C. S. Yoon, *Accepted to Colloids Surf.* (2006).
16. Thermal conductivity of PI-2610D is 3×10^{-6} °C^{-1} from the material data provided by Du Pont Electronics.
17. S. K. Lim, C. S. Yoon, C. K. Kim, and Y. -H. Kim, *J. Colloid Interface Sci*. **287**, 501 (2005).
18. J. F. Moulder, W. F. Stickle, P. E. Sobol, and K. D. Bomben, *Handbook of X-ray Photoelectron Spectroscopy*, p. 82, Physical Electronics, Inc., Minesota (1995).
19. G. H. Yu, L. R. Zeng, F. W. Zhu, C. L. Chai, and W. Y. Lai, *J. Appl. Phys.* **90**, 4039 (2001).
20. A. Galtayries and J. Grimblot, *J. Electron Spectrosc. Relat. Phenom.* **98-99**, 267 (1999).
21. B. D. Cullity, *Introduction to magnetic materials,* p. 157, Addison-Wesley publishing company, Massachusetts, (1972).
22. A. E. Berkowitz and K. Takano, *J. Magn, Magn. Mater.* **200**, 552 (1999).
23. J. Dai, J. -Q. Wang, C. Sangregorio, J. Fang, E. Carpenter, and J. Tang, *J. Appl. Phys.* **87**, 7397 (2000).
24. P Zhang, F. Zuo, F. K. Urban III, A. Khabari, P. Griffiths, and A. Hosseini-Tehrani, *J. Magn. Magn. Mater.* **225**, 337 (2001).
25. H. P. J. Wijn (ed.): *Magnetic Properties of Metals: d-Elements, Alloys and Compounds*, p. 38, Springer-Verlag, Berlin (1991).